JOURNAL OF GEOPHYSICAL RESEARCH, VOL. 114, D05106, doi:10.1029/2008JD010896, 2009

A multiproxy index of the El Niño–Southern Oscillation, A.D. 1525–1982

Karl Braganza,[1] Joëlle L. Gergis,[2] Scott B. Power,[1] James S. Risbey,[3] and Anthony M. Fowler[4]

Received 31 July 2008; revised 19 November 2008; accepted 12 December 2008; published 6 March 2009.

[1] An understanding of past variability in the El Niño–Southern Oscillation (ENSO), on interannual, interdecadal, and longer time scales, would be useful in assessing recent observed changes to ENSO and in determining the realism of climate model simulations. Using tree ring, coral, and ice core data, we reconstruct a proxy-based ENSO index between A.D. 1525 and 1982. Unlike most previous studies, which have drawn climate proxies from limited geographic regions, our network is Pacific basin–wide, using ENSO sensitive proxies from the western equatorial Pacific, New Zealand, the central Pacific, and subtropical North America. By considering multiple teleconnection regions, this network provides a more robust proxy ENSO signal. The common signal recorded in the multiproxy network has a high correlation with the Southern Oscillation Index (SOI), Niño 3.4 sea surface temperature (Niño3.4 SST), and a combined ocean-atmosphere ENSO index (CEI). The proportion of instrumental variance explained is 47% for the SOI, 48% for Niño3.4 SST, and 52% for the CEI. The proxy ENSO index also displays skill in reproducing warm and cold extremes of the SOI. The proxy ENSO index over the last 450 years shows considerable amplitude and frequency modulation in the 3–10 year band on multidecadal time scales. There is a relative reduction in the amplitude of high-frequency variability during the sixteenth, early seventeenth, and mid–eighteenth centuries. In contrast, high-frequency ENSO variability has increased over the last 200 years. Variability during the first half of the twentieth century is similar to that evident in the nineteenth century.

Citation: Braganza, K., J. L. Gergis, S. B. Power, J. S. Risbey, and A. M. Fowler (2009), A multiproxy index of the El Niño–Southern Oscillation, A.D. 1525–1982, *J. Geophys. Res.*, *114*, D05106, doi:10.1029/2008JD010896.

1. Introduction

[2] For many people, the most important impacts of climate change are related to changes in regional temperature and precipitation. However, the contribution of anthropogenic climate change to regional climate change is clouded by the presence of naturally occurring variability. For rainfall and temperature, a major source of this variability on 2–7 year time scales is the El Niño–Southern Oscillation (ENSO) [*Folland et al.*, 2001]. A major difficulty in the task of separating the anthropogenic signal from the background of natural, ENSO related variability is the relative brevity of the instrumental record, which covers a period of 100 years or less. Extended, multicentury reconstructions of ENSO can help us to assess how unusual 20th century variability in ENSO has been in a longer-term context.

[3] In comparison to reconstructions of global and hemispheric surface temperature, reconstructions of ENSO variability have received less attention [*Trenberth and Hoar*, 1996, 1997; *Crowley*, 2000; *Folland et al.*, 2001; *Mann*, 2003]. Paleoreconstructions of ENSO driven variability have generally relied on calibration techniques that relate ENSO sensitive variability in proxy indicators to an instrumental ENSO index, typically the Southern Oscillation Index (SOI) or Niño region sea surface temperature (SST). *Stahle et al.* [1998] produced a reconstruction of the December to February SOI for the period A.D. 1706–1977 using subtropical North American tree ring data. *D'Arrigo et al.* [2005] reconstructed December to February Niño 3 SST for A.D. 1525–1982 using an expanded and updated version of the *Stahle et al.* [1998] data. *Mann et al.* [2000] reconstructed October to March Niño3 SSTs for the period A.D. 1650–1980 using a restricted tropical subset of the *Mann et al.* [1998] global multiproxy data, while *Evans et al.* [2002] reconstruct spatial equatorial SSTs from coral stable isotope data. A review of recent approaches to

[1]Centre for Australian Weather and Climate Research, Bureau of Meteorology, Melbourne, Victoria, Australia.
[2]School of Earth Sciences, University of Melbourne, Melbourne, Victoria, Australia.
[3]Centre for Australian Weather and Climate Research, CSIRO, Hobart, Tasmania, Australia.
[4]School of Geography, Geology and Environmental Science, University of Auckland, Auckland, New Zealand.

0148-0227/09/2008JD010896$09.00

reconstructing ENSO from proxy records is provided by *Gergis et al.* [2006].

[4] Unlike surface temperature, which is a directly measurable quantity, ENSO is a coupled atmosphere-ocean climate phenomenon. How best to define and monitor ENSO is a question that has been posed for some time [*Rasmusson and Carpenter*, 1982; *Allan et al.*, 1996; *Trenberth*, 1997]. This question also presents difficulties for the reconstruction of ENSO from climate proxies. Proxy indicators of ENSO variability are diverse, and part of the difficulty in calibration arises from understanding what aspect of ENSO variability is being reflected in the proxies. For example coral proxies will register climate variability as a function of sea surface temperature and sea surface salinity, while tree ring segments may reflect variability in local rainfall, temperature or both. Of relevance to ENSO reconstructions calibrated to single (uncoupled) indices is the fact that ocean and atmosphere components of the system need not be synchronous in their timing or amplitude [e.g., see *Fairbanks et al.*, 1997; *Lyon and Barnston*, 2005; *Gergis and Fowler*, 2005]. Events that register strongly in some instrumental indices and proxies may be absent in others with obvious implications for proxy calibration. For example, *Gergis and Fowler* [2005] demonstrated that the identification of ENSO events was dependent upon the index employed. The presence of noise in the instrumental indices, such as the Madden Julian Oscillation (MJO) in the SOI [*Trenberth*, 1997], is also a confounding factor in the calibration of proxies.

[5] A second major problem in ENSO reconstruction arises because the strength of ENSO teleconnections is varied in both strength and persistence, and from region to region, for each event [*Allan et al.*, 1996; *Power et al.*, 1998; *van Oldenborgh and Burgers*, 2005]. In addition, the nature of the atmospheric and oceanic response to ENSO has been shown to be nonlinear (sign-dependent) in some locations [*Hoerling et al.*, 1997; *Power et al.*, 2006]. Hence, changes in ENSO climate teleconnections from event to event are also likely to confound reconstruction attempts, particularly if proxy data are restricted to isolated (single) regions. To date, the coverage of proxy data has been limited to predominately eastern Pacific teleconnection regions with limited representation of sites influenced by western Pacific teleconnections [*Stahle et al.*, 1998; *D'Arrigo et al.*, 2005]. A number of studies have suggested that a reconstruction of ENSO derived from a number of widely spaced regional proxies, with sufficient east and west Pacific representation, is more likely to be representative of ENSO than more restricted networks [*Baumgartner et al.*, 1989; *D'Arrigo et al.*, 1994; *Diaz and Pulwarty*, 1994; *Whetton and Rutherfurd*, 1994; *Evans et al.*, 2002; *Gedalof and Mantua*, 2002].

[6] In this paper we use a set of multiproxy indicators from locations that span a broader area of the Pacific basin than has been attempted previously. In this manner, we aim to represent climate signals from a range of different regions (tropics versus extra tropics, terrestrial versus marine environments) that have established responses to ENSO forcing. Specifically, the incorporation of new western Pacific proxies are introduced, including two high-quality tree ring records from New Zealand [*Fowler et al.*, 2000; *Fenwick*, 2003], and a well replicated Australian coral record from the Great Barrier Reef [*Hendy et al.*, 2003]. These records provide an important counterpart to the chronologies developed from eastern Pacific locations.

[7] We use the Pacific-wide network of ENSO sensitive proxies to identify a common, annually resolved ENSO signal, which we employ as a multicentury index of ENSO. Whereas previous studies have used regression-based calibration techniques to reconstruct the SOI or Niño region SST anomalies, our ENSO index is simply the time series of the leading principal component from the set of multiproxy indicators. In this way, the index is determined solely by ENSO-related covariability within the network and not by calibration to independent 20th century observed ENSO indices, as in studies that use the regression method.

[8] In this study, we compare our proxy ENSO index to the instrumental SOI, Niño3.4 SST and the coupled ocean-atmosphere ENSO index (CEI) of *Gergis and Fowler* [2005]. We also investigate the ability of our index to capture low-frequency (decadal and longer) variability through comparison with the Interdecadal Pacific Oscillation (IPO) and the low-frequency component of the SOI. Finally, we provide a brief discussion of ENSO variability since A.D. 1525.

2. Proxy Data

[9] A number of criteria are used for the selection of proxy records used in this study:

[10] 1. Each record is a seasonally or annually resolved published record from areas that have been identified by previous researchers as containing an ENSO signal [e.g., *Stahle et al.*, 1998; *Fowler and Boswijk*, 2003; *Hendy et al.*, 2003]. Coral records were limited to those with long record length and a significant correlation with ENSO over the 20th century as identified by the original researchers. The coral records used in this study are taken from the Great Barrier Reef [*Hendy et al.*, 2003], New Caledonia [*Quinn et al.*, 1998] and Rarotonga [*Linsley et al.*, 2000a].

[11] 2. Proxies are selected so that we maintain a network that spans the Pacific Basin (including eastern, western and central Pacific sites) and to ensure that individual regions are not overrepresented.

[12] 3. Each proxy in the network must have a continuous record. We have attempted to use records that are free of obvious inhomogeneities that may be expected to degrade the resultant reconstructions, though such discontinuities may still exist.

[13] Using these criteria we define two multiproxy networks: a larger network containing eight proxy sites (Figure 1) with continuous records from A.D.1727 to 1982, and a smaller network containing five continuous records from A.D. 1525 to 1982. The smaller network is a subset of the larger network that still maintains Pacific-wide coverage while extending the length of record by another 200 years.

[14] The five longest records (A.D. 1525 to 1982) are the kauri and pink pine tree ring chronologies from New Zealand (western Pacific, Southern Hemisphere), the Douglas fir and pinyon pine [*Stahle et al.*, 1998; *Cleaveland et al.*, 2003] tree ring chronologies from subtropical North America (eastern Pacific, Northern Hemisphere) and the Quelccaya ice core [*Thompson et al.*, 1984, 1985, 2000]

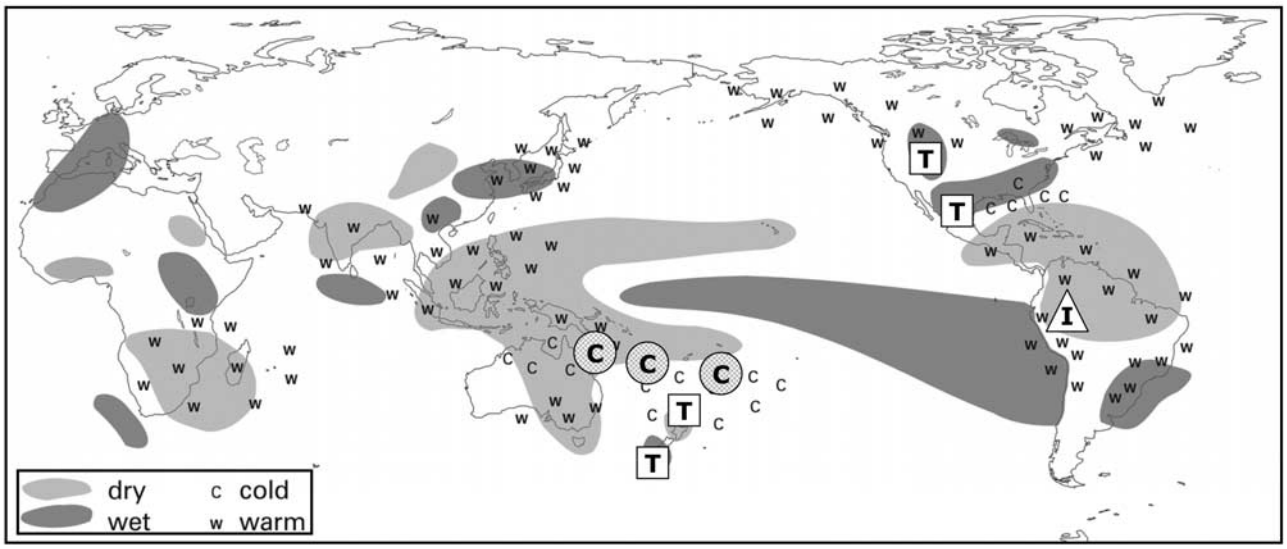

Figure 1. Location of proxy records used in this study shown with regard to El Niño teleconnection characteristics. Rainfall anomalies are represented in light gray shading (dry) and dark shading (wet). Temperature anomalies indicated by "c" (cool) and "w" (warm) annotation. "T" denotes tree ring chronologies (squares), "C" denotes coral sequences (circles), and "I" denotes ice core data (triangle). Note that R5 (1525) proxies are unshaded, and the R8 (1727) proxies are gray hatched. Details of each record are provided in Table 1. Note that the El Niño teleconnection base map is adapted from *Allan et al.* [1996].

from Peru (eastern Pacific, equator). The larger network (A.D. 1727 to 1982) contains the five records described above and three additional coral records. These records are the Great Barrier Reef and New Caledonia [*Quinn et al.*, 1998] coral records (western Pacific) and the Rarotonga [*Linsley et al.*, 2000a] coral record (central Pacific). It should be noted that the records used here are not a definitive list of ENSO sensitive proxies. There is scope for extending the proxy network to include proxies from other regions with well established ENSO teleconnections. The networks used here represent all of the records that satisfied the selection criteria and that were made available to us. Unfortunately we were unable to obtain suitable ENSO sensitive proxy records from Indonesia, China or India for this study.

[15] Since the proxy data used in this study are from various sources, some effort is made to ensure that the proxy time series are consistent in their temporal resolution. For each of the proxies used here, the "growth" signal (such as tree ring segment length) is recorded annually. In practice however, it is not always possible to obtain "raw" proxy time series, since most records are published and available only in processed format. This processing is typically high- or low-pass filtering of the annual signal. Here we ensure that the treatment of each tree ring chronology, and each coral sequence, is consistent.

[16] All tree ring chronologies used in this study are regional "master chronologies" that represent the mean of multiple core samples from multiple trees. For each species, these were produced using the method of *Fowler and Boswijk* [2003]. Tree ring chronologies are usually high-pass filtered to remove the low-frequency signals of biological origin (i.e., not related to climate variability) [*Cook and Peters*, 1981; *Fowler and Boswijk*, 2003]. Since such filtering is somewhat arbitrary, in terms of removing all of the lower-frequency variability, we seek to employ tree ring chronologies with little or no filtering, with the aim of retaining as much low-frequency climate information as possible. In practice (ensuring all records were subjected to the same data treatment), only tree ring chronologies filtered using a high-pass, 200 year cubic spline filter are available for this investigation. The preservation of variability on time scales less than 200 years from records with maximum length of 400 years should be sufficient for capturing any ENSO low-frequency variability.

[17] All coral and ice core records were filtered using a 3-year low-pass Gaussian filter, which attenuates year-to-year noise in the individual time series. This approach is consistent with studies [*Diaz and Markgraf*, 2000; *Goodwin et al.*, 2004; *Linsley et al.*, 2004; *Lough*, 2004] that use similar records to infer interannual and longer-scale climate variability from coral proxies.

[18] With the exception of the kauri, pink pine and the Great Barrier Reef records, all data have been obtained from the National Oceanic and Atmospheric Administration's World Data Center (NOAA WDC) for Paleoclimatology (details in Table 1). The kauri, pink pine and Great Barrier Reef chronologies are sourced via individual authors [*Fenwick*, 2003; *Fowler et al.*, 2004; *Gergis et al.*, 2005a, 2005b]. The reconstructions we present here will also be made available through the NOAA WDC for Paleoclimatology.

[19] The limitations and/or potential biases that are specific to each type of proxy are fairly well understood [*Jones and Mann*, 2004]. As mentioned, the temporal resolving power (i.e., seasonal, annual, decadal etc) is a key consideration in the reconstruction of ENSO variability. The proxy records used here resolve an annual signal

Table 1. Proxy Data Used in This Analysis

Proxy Record	Dates (A.D.)	Latitude, Longitude	Data Smoothing	ENSO Zone	Proxy Variable
Tree rings					
New Zealand kauri[a]	1525–2002	35–37°S, 173–175°E	200-year spline	West Pacific	total ring widths
New Zealand pink pine[b]	1525–1998	42–47°S, 167–174°E	200-year spline	West Pacific	total ring widths
Mexican Douglas fir[c]	1525–1998	19–30°S, 97–108°W	200-year spline	East Pacific	total ring widths
SW USA pinyon pine	1525–2000	33–37°S, 106–112°W	200-year spline	East Pacific	total ring widths
Coral					
Great Barrier Reef[d]	1612–1985	20°S, 147°E	3-year Gaussian	West Pacific	luminescence
New Caledonia[e]	1658–1992	22°S, 166°E	3-year Gaussian	West Pacific	δO^{18}
Rarotonga[f]	1727–1997	21°S, 159°W	3-year Gaussian	central Pacific	Sr/Ca
Ice					
Quelccaya ice core[g]	1525–1984	14°S, 71°W	3-year Gaussian	East Pacific	δO^{18}

[a] *Fowler et al.* [2000, 2004, 2008], *Gergis et al.* [2005a, 2005b], and *Fowler* [2008].
[b] *Fenwick* [2003].
[c] *Cleaveland et al.* [2003]; data from IGBP PAGES/WDC-A for Paleoclimatology Contribution Series 2002-004 by D. Stahle, M. Cleaveland, M. Therrell, B. Burns, G. Paull, and J. Villanueva-Diaz for Cerro Potosi, Creel International Airport, El Salto recollection, El Tabacote and Tomochi, Villareal, Mesa de Campanero, Las Tinajas, Cerro Baraja, and Los Angeles Sawmill (Mexico), 2002, available at http://www.ncdc.noaa.gov/paleo/; data from IGBP PAGES/WDC-A for Paleoclimatology Contribution Series 1994-003 by D. Graybill for Eagle Creek (Arizona, USA), 1994, available at http://www.ncdc.noaa.gov/paleo/; data from IGBP PAGES/WDC-A for Paleoclimatology Contribution Series 1992-012 by H. D. Grissino-Mayer and T. Swetnam for Oscura Peak White Sands Missile Range (New Mexico, USA), 1992, available at http://www.ncdc.noaa.gov/paleo/; data from IGBP Pages/WDC-A for Paleoclimatology Contribution Series 1993-021 by J. Dean for Paliza (New Mexico, USA) and Navajo Mountain (Utah, USA), 1993, available at http://www.ncdc.noaa.gov/paleo/; and data from IGBP Pages/WDC-A for Paleoclimatology Contribution Series 2003-094 by D. Grow for Coal Bench, Deer Springs Mesa, Lower Henderson Canyon, Round Valley Draw, Skutumpah Road #1, and Skutumpah Road #2 (Utah, USA), 2000, available at http://www.ncdc.noaa.gov/paleo/.
[d] *Hendy et al.* [2005].
[e] *Quinn et al.* [1999].
[f] *Linsley et al.* [2000b].
[g] *Thompson et al.* [1992].

that is registered during one particular season. On interannual time scales, ENSO proxies rarely capture more than 50% of instrumental variance. Furthermore, they are unable to register variance equally well across a number of frequency domains [*Bradley*, 1996]. For instance, the ability of tree ring climate proxies to faithfully capture low-frequency climate variability is potentially restricted because of physical limitations related to segment length. This issue is extensively discussed elsewhere [*Esper et al.*, 2002; *Hughes*, 2002; *Cook et al.*, 2004]. To address this, we compare our proxy-based ENSO index to instrumental ENSO indices at interannual and decadal time scales.

3. Instrumental ENSO Indices

[20] To quantify the accuracy of our proxy-based ENSO index, we compare it to the SOI and Niño3.4 SST and the *Gergis and Fowler* [2005] Coupled ENSO Index (CEI) index to represent ENSO over the instrumental period.

[21] The SOI time series (1871–2003) from the Australian Bureau of Meteorology is based on the Troup method [*Troup*, 1965]. This index is the standardized anomaly of the mean sea level pressure difference between Tahiti and Darwin, presented in standard deviation units around a mean of zero, with significant positive/negative departures representing La Niña/El Niño conditions.

[22] Data for the Niño 3.4 SST region (5°N–5°S, 120–170°W), for the period 1950–2003, has been obtained from NOAA's Climate Prediction Center. Pre-1950, we use the Trenberth and Stepaniak interpolation-based reconstruction of Niño3.4 SSTs, which is derived from the 1 degree gridded HadISST (Hadley Centre Sea Ice and Sea Surface Temperature) data set. It should be noted that spatial variability of SSTs prior to 1950 suffers from data quality issues in all existing maritime observational data sets [e.g., see *Power and Colman*, 2006].

[23] The CEI is a composite index based on the oceanic (Niño3.4 SST) and atmospheric (SOI) indices described above. Anomalies expressed in either Niño3.4 SST or the SOI alone (and therefore perhaps indicative of decoupled or out of phase changes) are maintained in the CEI, while fully coupled ocean-atmospheric anomalies result in an amplification of the index.

4. Methods

[24] A large proportion of the total variability, on any given time scale, in individual paleoclimate records is due to nonclimatic factors. For example, biological processes account for a significant proportion of lower-order autocorrelation in tree ring chronologies. Extracting the climate signal from this background variability (noise) in a single paleoclimate record is a difficult task. Previous studies have taken a similar conceptual approach to developing ''transfer functions'' that relate proxy records to ENSO. Almost all have sought to ''calibrate'' individual proxy records, or multiproxy networks, using multivariate regression against instrumental observations.

[25] For instance, *Stahle et al.* [1998] use ''PC-based regression,'' whereby leading Empirical Orthogonal Functions (EOFs) from a multiproxy data set are regressed against the instrumental SOI over the 20th century. This regression model is then used to hindcast SOI variability prior to the 20th century. *Mann et al.* [1998, 2000], and *Evans et al.* [2002], take the ''inverse'' approach to calibrating their proxy data. They first decompose 20th century tropical Pacific SSTs into multiple, spatial EOFs. A calibration model is then defined by regressing individual proxy records from a multiproxy data set onto the time series of the leading observed modes. Whether one is regressing the time series of leading multiproxy modes of variability onto 20th century climate indices or one is training the proxy

data to spatially determined modes of 20th century observed variability (inverse method), an underlying assumption is made that fundamental relationships between the proxy indicators and the real climate during the 20th century is similar to climate of the past.

[26] In this study we take a relatively simple approach to defining an ENSO index from a multiproxy network. We reason that an appropriately chosen proxy ENSO network, following the spatial distribution requirements we outlined earlier, should be robust enough to resolve a common mode of covariability that directly represents basin-wide ENSO. This "proxy ENSO" is not calibrated to 20th century observations. Rather, it is an index that is comparable to one or more instrumental ENSO indices while not explicitly representing any. While the main purpose of any climate reconstruction is to provide historic context for current climate variability, this does not necessarily require that the proxy climate record be directly calibrated to the instrumental record. This is particularly so if the proxy climate record continuously spans past and present climate. In the case of hemispheric and global mean temperature, expressing past proxy-derived temperature variability in Kelvin is useful for the tangible assessment of recent and future, projected changes. However, for ENSO, such calibration to instrumental indices is less meaningful. This is because ENSO phases are not directly measurable quantities. Rather, multiple indices exist to describe the state of the coupled ocean-atmosphere system that comprises ENSO, each with well documented attributes and deficiencies. Further, such indices are often expressed as standardized (unitless) magnitudes. As such, our proxy ENSO index simply provides another measure of ENSO variability, with a continuity of record prior to the instrumental period.

[27] To decompose the basin-wide multiproxy network into leading modes of covariability, we use Empirical Orthogonal Function (EOF) analysis. The EOF analysis is an effective filter of nonclimate related noise in the network, since this background noise has very short spatial scales and is therefore not present as variability that is synchronous or coherent across the whole network. This fact is further exploited by selecting a multiproxy network where noise due to internal biological processes would be expected to have no relationship across the diverse group of indicators. Any common signal in the network (most likely to be climate related) will be represented by the lower-order eigenvectors, while uncorrelated noise is separated into higher-order eigenvectors. The orthogonality requirement of EOF analysis means that the ENSO signal should be isolated by a single leading eigenvector (or EOF), the time series of which represents our "proxy ENSO" index. In effect, the entire "calibration" is performed by simply applying the EOF analysis and dependent upon the selection of an appropriate network.

[28] We represent the proxy network described in section 2 as the matrix $\boldsymbol{X}$ dimensioned (M,N), corresponding to a time series of N values at M locations. Following *Kutzbach* [1967], we define the correlation matrix $\boldsymbol{R}$(M,M) of the proxy network as;

$$R = (N-1)^{-1} Z'^{T} Z', \tag{1}$$

where $\boldsymbol{Z}$ represents the proxy matrix $\boldsymbol{X}$ linearly transformed into standardized (unit variance) deviations, we define a set of orthonormal basis vectors ($\boldsymbol{E_j}$, j = 1, 9) or eigenvectors;

$$R\widetilde{E}_j = [\lambda_j]\widetilde{E}_j.., \tag{2}$$

where λ_j (eigenvalue) is the jth diagonal element of the transpose of the correlation matrix $\boldsymbol{R}$.

[29] Each eigenvector (EOF) represents an orthogonal mode of covariability in the proxy data set $\boldsymbol{X}$, with the lower-order eigenvectors explaining the largest fraction of the total variance. Time series of each EOF are generated by projecting each eigenvector onto $\boldsymbol{X}$ at each time step, representing the amplitude of each mode through time. The relevant mode relating to ENSO is determined through comparison with the SOI over the 20th century. Hence, the time series of this EOF may be considered as a "proxy ENSO" index that is analogous to instrumental ENSO indices. In the multiproxy network used here, ENSO variability is represented by the leading EOF and no other modes were found to have any association with instrumental ENSO indices.

[30] As outlined in section 2, the signal of ENSO in each proxy is registered annually during a particular season. For tree rings, growth seasons typically last three to six months and occur at different times of the year, depending on the type of proxy and where it is located. This is an issue for Southern Hemisphere tree rings, where growth seasons can be spread over two calendar years, corresponding to the Southern Hemisphere summer. Dating convention determines which year the growth season is recorded in, typically the previous year if the growth season covers two calendar years. Hence, prior to calculating the correlation matrix for the proxy network, each time series was adjusted such that the appropriate growth seasons are annually synchronous. In practice, only the kauri record from New Zealand requires adjustment by a 1 year lag to ensure it is synchronous with all other records. Two proxy ENSO indices are defined, one using the long (A.D. 1525–1982) network of five proxies (hereafter referred to as R5) and the other from (A.D. 1727–1982) using the extended network of eight proxies (hereafter referred to as R8). Note that R5 is a spatial subset of R8 and hence is not independent.

[31] *Braganza et al.* [2008] provide more details of the EOF method in its relation to defining a common proxy climate signal. This material is provided as auxiliary material to this paper.[1] Using synthetic data, *Braganza et al.* [2008] compared the approach of simply taking the leading EOF from a multiproxy network with various regression based calibration or reconstruction techniques found commonly in the literature. They show that this simple approach leads to skill in simulating ENSO variability in independent data at comparable levels to previous studies. They also demonstrate that the EOF method of signal extraction used here provides a simple means of removing non-ENSO related noise from proxy records. Further, *Braganza et al.* [2008] (see auxiliary material) also used synthetic data to examine several "preprocessing" techniques that are used

[1] Auxiliary materials are available in the HTML. doi:10.1029/2008JD010896.

Table 2. Variance Explained in the First Four EOFs of Multiproxy Data[a]

Multiproxy Data Set	EOF1	EOF2	EOF3	EOF4
R8 (1727–1982)	23	15	13	12
R5 (1525–1982)	30	21	19	17

[a]Variance is in %.

commonly in regression based calibration, namely, high- and low-pass filtering, prewhitening and detrending of individual proxy chronologies prior to the calculation of the covariance matrix. In regression based studies, such preprocessing may be required to remove nonclimate related noise and ensure that the resultant model is built upon the relevant climate signal alone. For the simple EOF method used here, they found that prefiltering, prewhitening or detrending of the data leads to no appreciable improvement in the fidelity of the extracted climate signal.

[32] In terms of preserving as much low-frequency (decadal or greater) variability as possible, the EOF method works best with raw (unfiltered) proxy data. We also conclude that by not calibrating the proxy time series against 20th century observations, we may expect greater homogeneity over the entire length of the record, since there is less likelihood that the index is tuned to the signal of 20th century variability. Importantly, this approach may therefore provide more certain temporal continuity for assessing relative changes in the signal over time.

5. Proxy ENSO Index

[33] We compare the time series of our proxy ENSO index to the time series of instrumental ENSO indices over the 20th century. Comparisons are made using temporal correlation, correspondence in the spectral domain, and skill in the ability of the proxy ENSO index to simulate threshold-based El Niño and La Niña events.

Table 3. Correlations Between the Annual R8 EOFs 1–4 and 11-Month Mean SOI, 5-Month Mean Niño3.4, and Monthly CEI Centered on July and October of the Preceding Year and January, April, and July of the Concurrent Year for the Period 1871–1982[a]

	July (t − 1)	October (t − 1)	January (t = 0)	April (t = 0)	July (t = 0)
EOF1					
CEI	**0.54**	**0.67**	**0.72**	**0.63**	**0.40**
SOI	**0.51**	**0.62**	**0.69**	**0.57**	0.38
N3.4	0.12	**0.49**	**0.65**	**0.70**	**0.59**
EOF2					
CEI	0.00	0.05	0.00	0.05	0.02
SOI	0.02	0.01	0.01	0.05	0.06
N3.4	0.16	0.02	0.06	0.01	0.13
EOF3					
CEI	0.16	0.20	0.18	0.16	0.17
SOI	0.14	0.16	0.17	0.14	0.11
N3.4	0.12	0.17	0.20	0.17	0.16
EOF4					
CEI	0.03	0.06	0.08	0.09	0.18
SOI	0.05	0.05	0.11	0.16	0.22
N3.4	0.01	0.01	0.06	0.06	0.03

[a]Bold values represent correlations significant at the 0.01 two-tailed level. N3.4, Niño3.4.

[34] Here we present the correlation (R) and the proportion of common variance explained (R^2) between the proxy ENSO index and observed indices of ENSO. Any close association between our index and instrumental indices over the 20th century would imply that the index is a suitable proxy for ENSO variability. Table 2 shows variance explained by the leading four EOFs from both of the multiproxy networks, R5 (1525 to 1982) and R8 (1727 to 1982). While most of the variance in the proxy records is evenly spread across the four leading modes of variability, only the first mode is correlated with the instrumental ENSO indices (Table 3). The uniform distribution of the variance in multiple directions highlights the degree of noise on interannual to multidecadal time scales that exists within the paleodata.

[35] The geographic distribution of proxies is obviously an important component in accurately capturing ENSO-related variability. Table 4 shows the relative loading (first eigenvector) for each of the proxy chronologies from the 1727–1982 network and their lead/lag correlation with the associated R8 (EOF1) time series. The loadings represent a measure of coherent variability associated with the direction of the leading EOF and hence indicate which sites contribute most to the overall variance within this mode. The variance associated with R8 is dominated by covariability in all of the tree ring chronologies, the Quelccaya ice core and the Rarotonga coral record. Importantly, the resolved signal is not dominated by a particular hemisphere and seems to capture a coherent, basin-wide signal.

[36] Correlations between the annual R8 proxy ENSO (EOF1) and the SOI for various different SOI averaging periods are shown in Table 5. The significance of these correlations may be judged according to a null hypothesis of no association between the proxy records and ENSO. Using this measure, correlations of greater than 0.25 in magnitude are statistically significant at the 0.01 level (two-tailed). The proxy ENSO index has its highest association with the SOI from around August of the previous year to March of the concurrent year. This result is consistent with previous studies which show that proxy association with ENSO indices is greatest in December through to May [see, e.g., *Stahle et al.*, 1998].

[37] Table 3 shows the correlation between the leading four EOFs from R8 and the SOI, CEI and Niño3.4 SST. The

Table 4. Principal Component Loadings (Eigenvectors) and Annual Correlation Between Individual Proxy Chronologies and PC1 and PC2 Time Series Shown With Lead and Lag Time of 1 Year[a]

Individual Proxy Records Represented in the R8 Multiproxy Data Set	EOF Loading (Eigenvector)	Correlation		
		t − 1	t	t + 1
New Zealand kauri	0.34	0.04	0.46	0.10
New Zealand pink pine	−0.39	−0.07	−0.53	−0.23
Mexican Douglas fir	0.53	0.20	0.71	0.17
SW USA pinyon pine	0.40	0.18	0.54	0.04
Quelccaya ice core	0.33	0.33	0.45	0.27
Great Barrier Reef	−0.18	−0.11	−0.24	0.07
Rarotonga	0.34	0.22	0.46	0.29
New Caledonia	0.18	0.14	0.25	0.23

[a]Correlations above 0.25 are statistically significant at the 0.01 level (two-tailed) assuming a null hypothesis of no association.

Table 5. Correlations Between the Annual R8 EOF1 and the SOI for the Period 1877–1982 (106 Years) for Various Different SOI Averaging Periods[a]

	Number of Months											
Start Month	1	2	3	4	5	6	7	8	9	10	11	12
Apr	−0.087	−0.175	−0.323	−0.406	−0.430	−0.462	−0.489	−0.525	−0.556	−0.584	−0.607	−0.621
May	−0.224	−0.389	−0.463	−0.472	−0.499	−0.523	−0.557	−0.586	−0.612	−0.632	−0.643	−0.661
Jun	−0.445	−0.503	−0.499	−0.522	−0.545	−0.578	−0.607	−0.631	−0.650	−0.658	−0.676	−0.668
Jul	−0.493	−0.476	−0.504	−0.532	−0.573	−0.607	−0.634	−0.653	−0.663	−0.680	−0.670	−0.678
Aug	−0.403	−0.466	−0.509	−0.561	−0.604	−0.636	−0.657	−0.668	**−0.686**	−0.672	−0.679	**−0.678**
Sep	−0.480	−0.521	−0.577	−0.624	−0.657	−0.676	−0.686	**−0.700**	−0.682	**−0.686**	**−0.682**	−0.655
Oct	−0.493	−0.577	−0.640	−0.675	−0.694	−0.698	**−0.707**	−0.683	−0.683	−0.673	−0.641	−0.606
Nov	−0.551	−0.642	**−0.681**	**−0.701**	**−0.699**	**−0.703**	−0.669	−0.666	−0.652	−0.615	−0.577	−0.565
Dec	−0.572	−0.642	−0.675	−0.674	−0.679	−0.639	−0.634	−0.614	−0.572	−0.531	−0.520	−0.513
Jan	−0.561	**−0.652**	−0.638	−0.649	−0.602	−0.594	−0.570	−0.526	−0.484	−0.476	−0.471	−0.451
Feb	**−0.589**	−0.577	−0.601	−0.543	−0.536	−0.510	−0.463	−0.422	−0.419	−0.417	−0.397	−0.378
Mar	−0.411	−0.512	−0.449	−0.450	−0.430	−0.389	−0.352	−0.357	−0.359	−0.343	−0.327	−0.308
Apr	−0.492	−0.387	−0.391	−0.372	−0.332	−0.298	−0.310	−0.316	−0.301	−0.286	−0.270	−0.254
May	−0.166	−0.243	−0.258	−0.233	−0.213	−0.237	−0.251	−0.242	−0.231	−0.217	−0.203	−0.196
Jun	−0.255	−0.260	−0.227	−0.203	−0.232	−0.248	−0.237	−0.225	−0.210	−0.196	−0.189	−0.176

[a]The vertical axis shows the starting month of the SOI averaging period, starting in April the year before the annual EOF1 value (t − 1) through to June of the concurrent year. The horizontal axis shows the number of months in the SOI averaging period, ranging from 1 month to 12 months. Bold values show the highest correlation for each averaging period.

CEI is a monthly, combined land-ocean index composed of an 11-month mean SOI and an inverted 5-month mean of Niño 3.4 SSTs. The use of 11-month mean SOI and 5-month mean SST to represent ENSO follows from *Trenberth and Hoar* [1996, 1997] and *Allan et al.* [2003] for the SOI and from *Trenberth* [1997], *Trenberth and Stepaniak* [2001] and *Hanley et al.* [2003] for Niño3.4 SST (for further details see *Gergis and Fowler* [2005]). For ENSO indices, taking temporal averages that are longer than three months may be expected to remove some of the influence of short-term weather events such as the MJO on the monthly SOI. Table 3 shows the correlation between the annual EOFs and the CEI for July and October of the previous year and January, April and July of the concurrent year. To allow for similar comparison, we also correlate the leading four EOFs with the 11-month mean SOI and the 5-month mean Niño3.4 SST centered on July, October, January and April as previously. The CEI displays similar characteristics to the SOI, with the highest association with EOF1 occurring for averages centered on the Southern Hemisphere summer months. For Niño3.4 SST, the relationship with EOF1 persists for later in the concurrent year. There is little or no association between any of the instrumental indices and proxy EOFs 2–4 for the R8 network.

[38] The proxy ENSO index explains a high proportion of variability in all three of the ENSO indices, the closest association occurring with the CEI coupled index. Table 6 expresses the associations described in Table 3 as proportion of variance explained for proxy ENSO R5 and R8 and each of the ENSO indices. Comparison between R5 and R8 indicates that the inclusion of more records in the network improves the subsequent reconstruction in terms of correspondence with 20th century ENSO. The proportion of instrumental variance explained by R5 and R8 compares well with previous efforts at ENSO index reconstruction. For example, *Mann et al.* [2000] were able to resolve 34–42% of October to March instrumental Niño 3 SST using three EOFs. *Stahle et al.* [1998] capture a maximum of 53% for December to February instrumental SOI. More recently, *D'Arrigo et al.* [2005] resolve between 43 and 52% of Niño 3 DJF SST. Here, the R8 index explains 48% of January centered 11-month mean SOI variability, 53% of January CEI variability and 49% of April centered 5-month mean Niño3.4 SST. R5 explains 42% of 20th century CEI variability. Figure 2 shows 20th century R8 scaled to instrumental SOI, CEI and Niño3.4 SST. Residuals from the reconstructions (not shown) are normally distributed and free of significant autocorrelation.

[39] Next we compare the spectral characteristics of the instrumental SOI and the proxy ENSO index. Power spectra are calculated from anomaly data (mean removed) and smoothed using multiple passes of a centrally weighted, moving three-point window (1-2-1 weighting) across the frequency domain. The background red noise spectrum is estimated from the theoretical AR1 or Markov process noise [*Gilman et al.*, 1963; *Torrence and Compo*, 1998]. The significance of spectral peaks relative to background noise is estimated from the AR1 noise spectrum and the χ-squared/degrees of freedom distribution [*Bath*, 1974], with the degrees of freedom dependent on the size of the

Table 6. Proportion of Common Variance Explained (R^2) Between Reconstructions and 11-Month Mean SOI, 5-Month Mean Niño 3.4 SST, and Monthly CEI, Centered on July and October of the Preceding Year and January, April, and July of the Concurrent Year for the Period 1871–1982

ENSO Index	Proportion Variance (%) Explained: R8	Proportion Variance (%) Explained: R5
CEI		
Jul (t − 1)	29	23
Oct (t − 1)	44	36
Jan (t = 0)	53	43
Apr (t = 0)	40	38
SOI		
Jul (t − 1)	26	19
Oct (t − 1)	38	30
Jan (t = 0)	48	38
Apr (t = 0)	33	29
Niño3.4 SST		
Oct (t − 1)	24	21
Jan (t − 1)	42	34
Apr (t = 0)	49	40
Jul (t = 0)	35	34

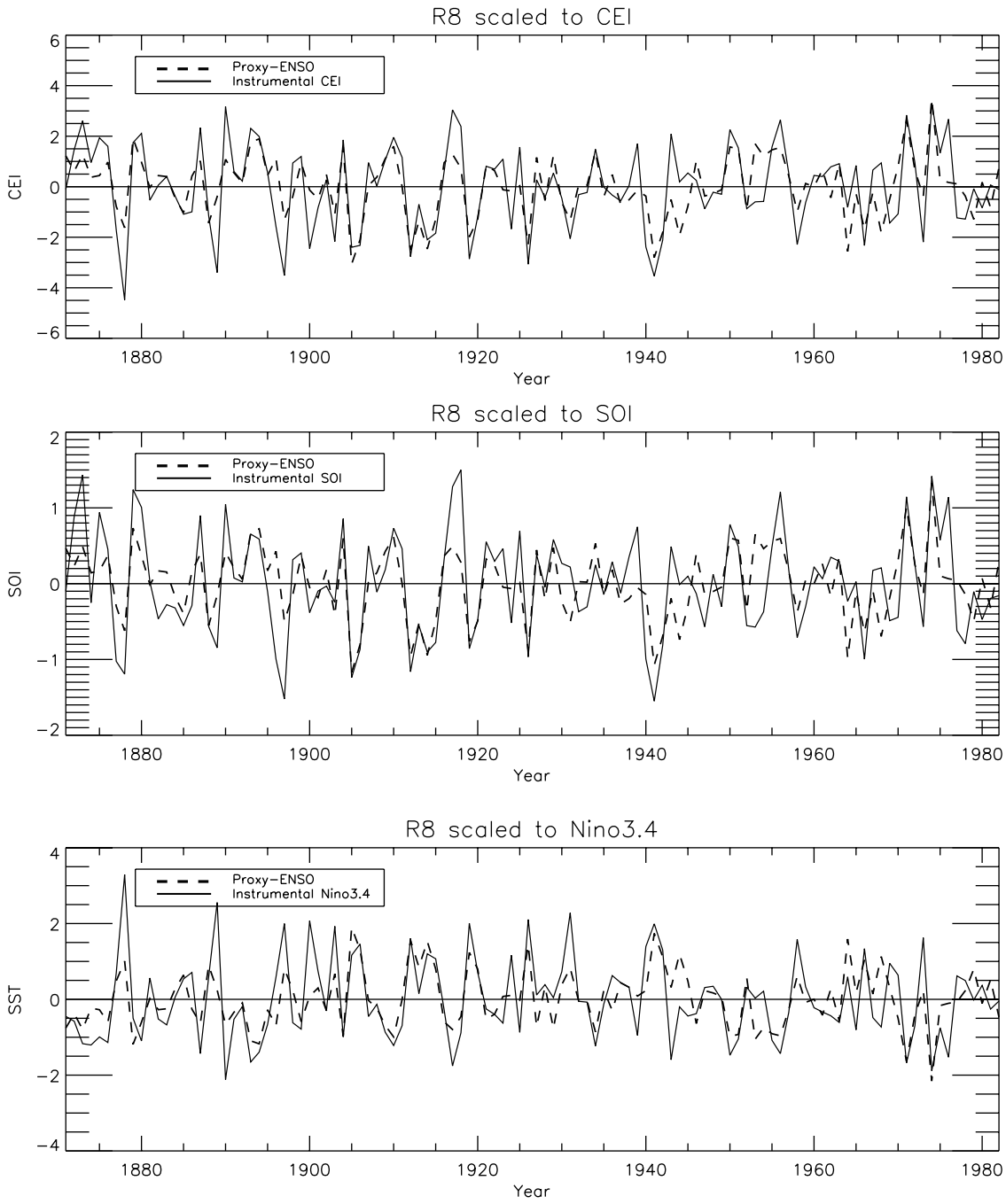

Figure 2. Time series of R8 proxy ENSO scaled to instrumental January CEI, September–August mean SOI, and February–June mean Niño3.4 SST over the period 1871–1982.

effective bandwidth after smoothing. Results in this study were compared with other methods of power spectra and background noise estimation, most notably the multitaper method [*Mann and Lees*, 1996], and found to be similar.

[40] Spectral power for the instrumental November–April mean SOI from 1877 to 1982, compared with R8 and R5 over the same period, is shown in Figure 3. Power spectra for Niño3.4 SST and the CEI (not shown) are very similar to the SOI. From Figure 3, peaks in spectral power for the SOI occur at ~2.9, ~3.5 and ~6.2 year frequencies. Spectral analysis of R8 for the period A.D. 1727–1982 is shown in Figure 4. While no direct comparison can be made between Figures 3 and 4 (since spectral results are sensitive to the time period), R8 over the last 300 years contains many of the spectral signals seen in the 20th century SOI, as well as greater low-frequency variability. In general, the reconstructions reproduce the 20th century spectral signal well, with cross-spectral analysis (Figure 3b) indicating significant coherence at observed ENSO frequencies.

6. ENSO Event Reconstruction

[41] Previous researchers have used paleoclimate and historical evidence to document past El Niño and La Niña

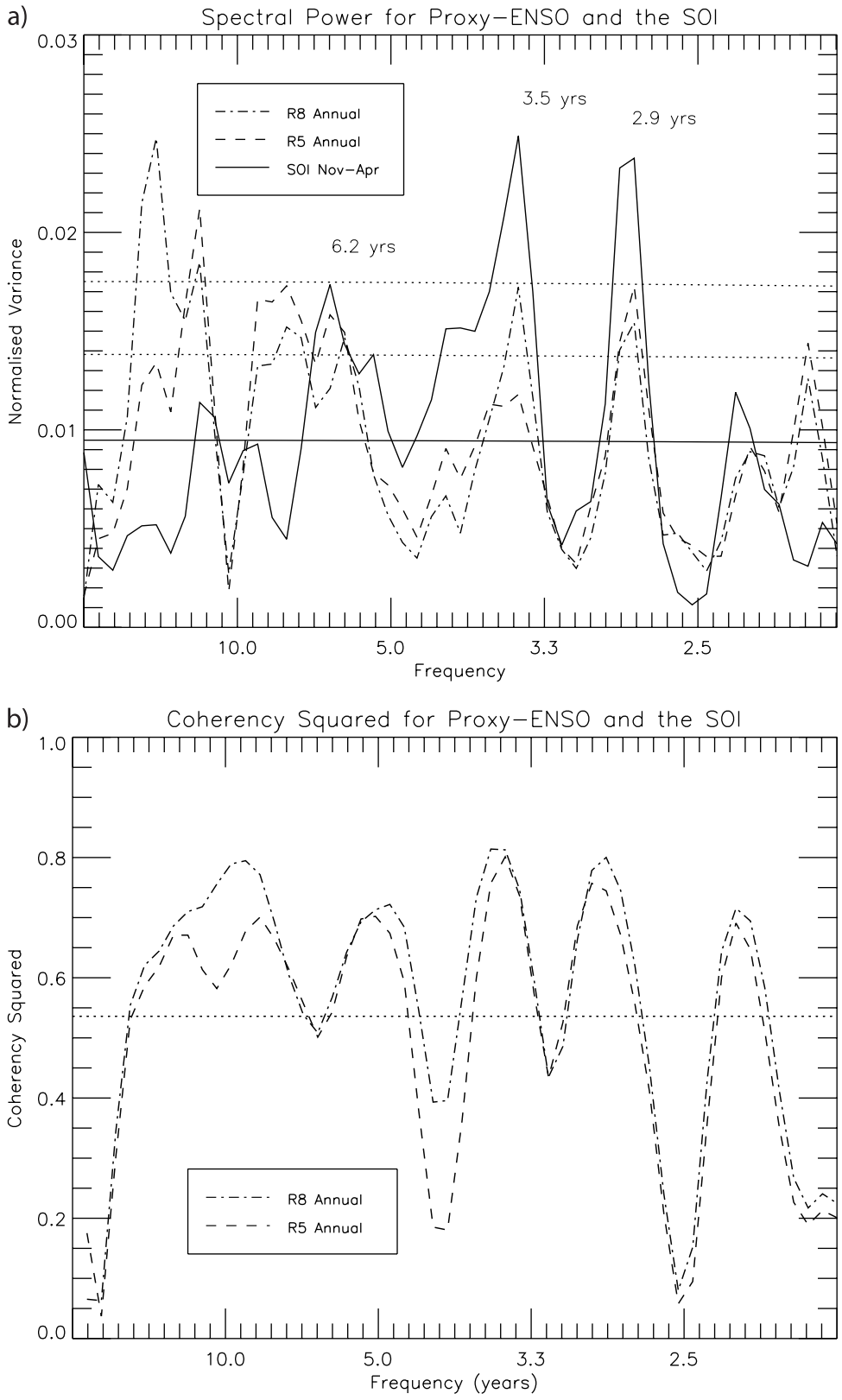

Figure 3. (a) Power spectrum for instrumental November–April mean SOI and annual proxy ENSO indices R5 and R8 for the period 1871–1982. Significance at the 90% and 95% (dotted lines) level is indicated relative to estimated background AR1 noise for the instrumental SOI. Effective bandwidth after smoothing = 2.66/N cycles/a. (b) Coherency squared for proxy ENSO indices R5 and R8 and instrumental November–April mean SOI for the period 1877–1982. 95% significance is indicated (dotted line).

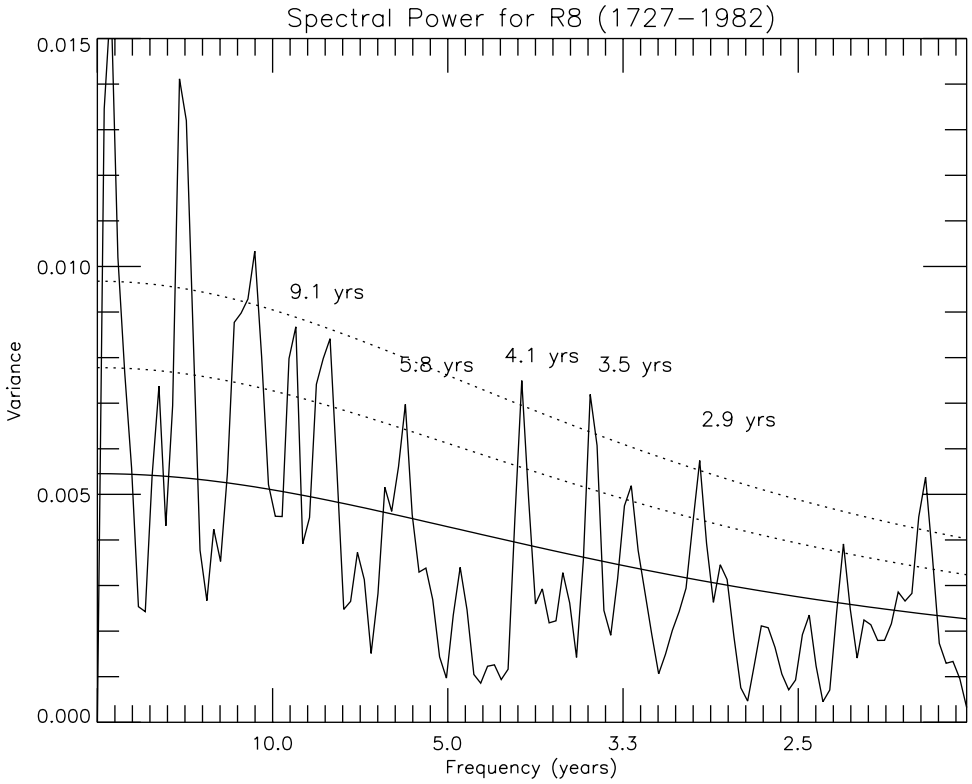

Figure 4. Power spectrum (unnormalized variance) for R8 proxy ENSO index (EOF1) for the period 1727–1982. Significance at the 90% and 95% (dotted lines) level is indicated relative to estimated background AR1 noise (solid line). Effective bandwidth after smoothing = 3.2/N cycles/a.

events [e.g., *Quinn and Neal*, 1992; *Whetton and Rutherfurd*, 1994; *Ortlieb*, 2000; *Garcia-Herrera et al.*, 2008]. Similarly, studies that have attempted to reconstruct continuous (annual) indices of ENSO have also sought to assess how well their records reproduce individual events. *Stahle et al.* [1998] (SOI) and *Mann et al.* [2000] (Tropical SSTs) use a single (one) standard deviation threshold to define and compare El Niño and La Niña events in their records and the observations.

[42] A number of factors affect the ability of proxy-based ENSO indices to capture signature ENSO events. One potential limitation is nonlinearity in the relationship between ENSO and the proxy ENSO index for large amplitude events. However, Figure 5 shows that there is little evidence of such nonlinearity in our proxy ENSO index. In Figure 6, we compare the 10-year moving mean standard deviation for R8 and observed November–April mean SOI. Both Niño3.4 SST and the CEI exhibit similar, decadal changes in variance to the SOI.

[43] The type of instrumental index used to identify warm and cold events can also be expected to affect comparisons between proxy ENSO and observed ENSO. Here we choose to use the SOI to identify observed events, principally because it provides a higher-quality record than SST indices over the earlier part of the 20th century. Choosing an appropriate temporal average for the SOI is an important consideration. While the proxy ENSO index has its highest association with the SOI from around August through to April, this is not the most suitable period for identifying ENSO events from an atmospheric circulation index. For this reason we use the June–November monthly mean SOI to identify El Niño and La Niña events in the observations. This period is traditionally associated with the peak maturity of El Niño events in the tropical circulation [e.g., see *Rasmusson and Carpenter*, 1982]. As mentioned previously, taking a six month average of the SOI may be expected to remove any contribution from weather events. On the basis of Table 5, the proxy ENSO index has its highest association with June–November SOI in the previous calendar year. R5 has a correlation of 0.50 with June–November SOI of the previous year, while R8 has a correlation of 0.58.

[44] To assess the accuracy of discrete event capture (the ability to record warm and cold phase events) in the proxy ENSO index, we follow the approach of previous studies [*Stahle et al.*, 1998; *Mann et al.*, 2000] and use a single (one) standard deviation threshold to define El Niño (negative SOI anomaly) and La Niña (positive SOI anomaly) events from both R5 and R8, and from the June–November SOI. For the list of instrumental events, we also indicate a number of marginal or weak events, that fail to meet the one standard deviation threshold but have been documented elsewhere (for example the Australian Bureau of Meteorology's list of El Niño and La Niña events that is available on the World Wide Web). These results are summarized in Figure 7 for the period A.D. 1876 to 1982 (the period with the highest-quality instrumental observations). First we concentrate on El Nino events identified since 1876. Twenty one events (including five weak events) are recorded in the SOI over this time period. Five of these occur prior to the

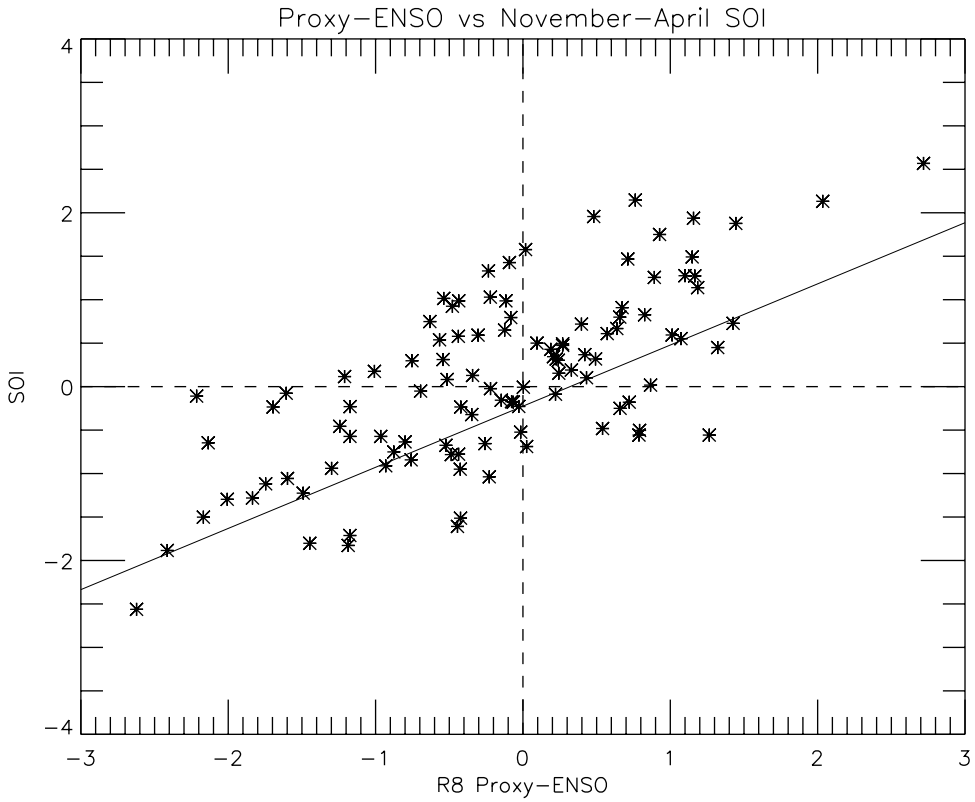

Figure 5. Scatterplot of proxy ENSO index (EOF1) R8 with observed mean November–April SOI for 1877–1982.

20th century, 1877, 1881, 1885, 1888 and 1896. The first and last of these events, in 1877 and 1896, are captured by both R5 and R8. The events of 1885 and 1888 are registered in the preceding year by the proxies, perhaps reflecting the strongly negative SOI prior to June of that year. The event of 1881 is not present in the reconstructions.

[45] Sixteen events are identified in the period 1900 to 1982. Six of these events are registered in the proxy ENSO indices, those of 1905, 1911, 1919, 1925, 1940 and 1965. The event of 1977 is registered in the following year in both R5 and R8 reflecting a persistently negative SOI into December through February of 1977–1978. Two periods of continuously negative SOI, recorded from 1940 to 1943 and 1963–1966, are captured by both R5 and R8. R5 registers the weak El Niño events of 1902, 1913, 1951 and 1957, which are not identified by the one standard deviation threshold in the SOI. Conversely, the moderate, short-lived El Niño events of 1923 and 1946 are recorded by the one standard deviation threshold in the SOI but are not registered by the proxy indices. The event of 1972 marginally fails to reach the threshold value in the proxy indices. This event registered strongly in Indonesia and New Guinea [*Quinn et al.*, 1978; *D'Arrigo et al.*, 1994], and we again note that the inclusion of proxies from this

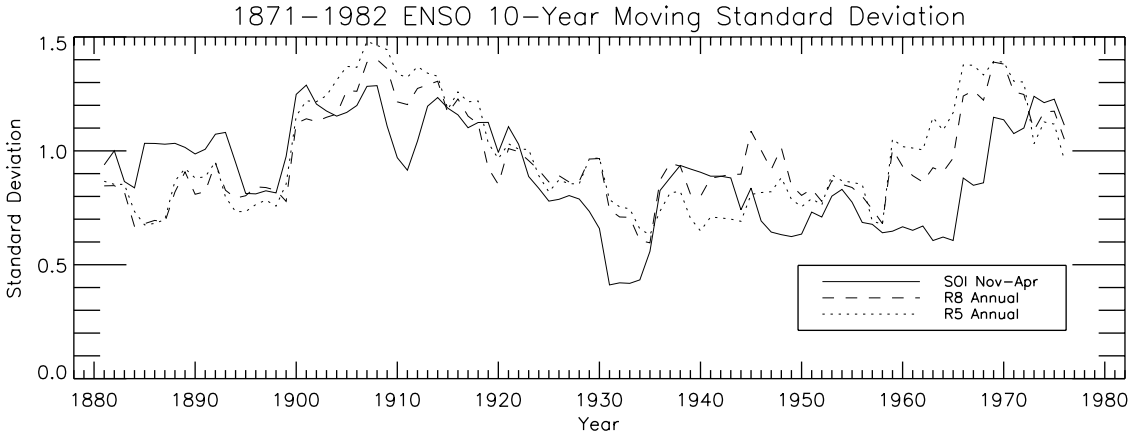

Figure 6. Ten-year moving variability (standard deviation) for instrumental November–April mean SOI and proxy ENSO indices R5 and R8 for the period 1877–1976.

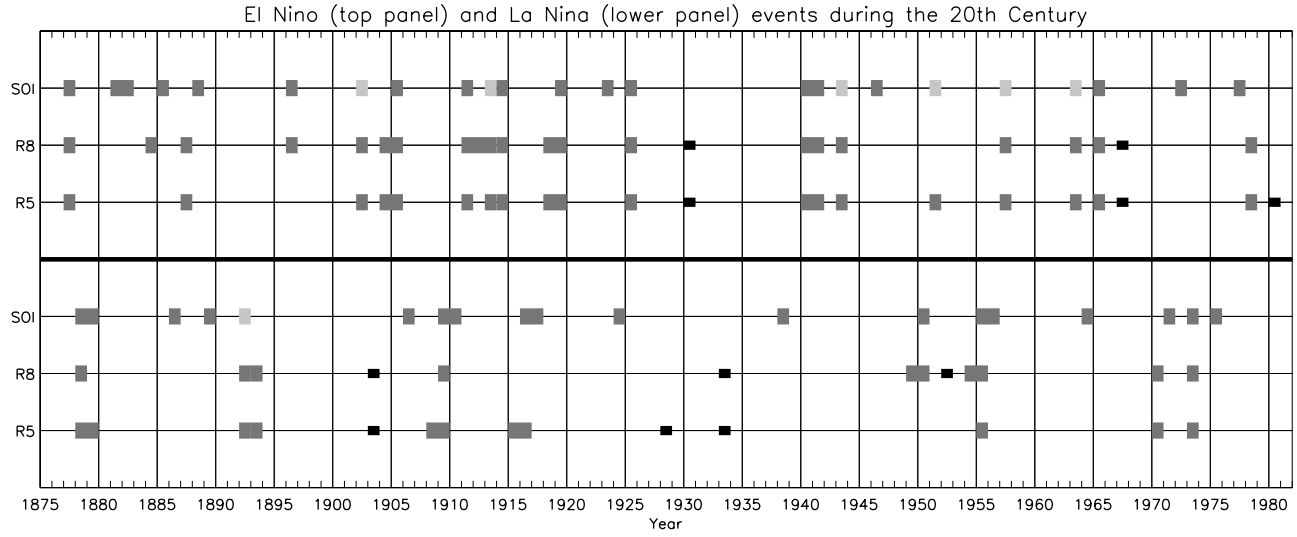

Figure 7. (top) El Niño and (bottom) La Niña events recorded since 1875 in the SOI, R5, and R8 proxy ENSO indices. Events are represented as solid dark gray squares. Events are defined as episodes (years) which are less than a single standard deviation (El Niño) or greater than a single standard deviation (La Niña) relative to variability from 1875 to 1982 (SOI), 1525–1982 (R5), and 1727–1982 (R8). Light gray squares represent weak events that did not reach the threshold in the SOI. Smaller black squares represent "false positive" events in the R5 and R8 proxy ENSO indices.

region would potentially improve the reconstruction. False El Niño events (ones not recorded in the SOI or elsewhere) are reproduced by R5 in 1930 and 1980 and by both R5 and R8 in 1967.

[46] Fifteen La Niña events (including one weak event) are identified from the SOI from 1876 to 1982. Prior to the 20th century R5 and R8 correctly identify the event of 1878. The event of 1889 is present in the proxies, but marginally fails to reach the threshold value. Both proxies fail to register the recorded event of 1886. A possible weak event in 1892–1893 is also identified by both indices. During the 20th century, strong La Niña events were correctly identified in 1909, 1916, 1950 (R8), 1955 (R8) and 1973. A short-lived positive anomaly in the SOI during 1903–1904 is registered as an event in both R5 and R8. The event of 1971 is registered in the preceding year in the proxy index, reflecting concurrent positive (but below the threshold) SOI anomalies from that period. Events in 1906, 1924, 1938, 1975 and a weak La Niña during 1964 are all missed by the proxies. False positive identification occurs in 1928 (R5), 1933 and 1952 (R5). There is also a tendency for the proxies to register the year preceding a La Niña as above the standard deviation threshold, even when the observed SOI does not display sustained positive anomalies. This occurs for the years 1908, 1915, 1949 (R8) and 1969–70.

[47] In general, one may expect differences in the ability of paleoclimate indicators to accurately register El Niño and La Niña events. Nonlinearity in ENSO teleconnections has been noted by previous researchers [*Hoerling et al.*, 1997; *Power et al.*, 2006]. For example, *Power et al.* [2006] show that the magnitude of La Niña SST anomalies is closely correlated with the magnitude of the response in area-averaged Australian rainfall changes, whereas the magnitude of El Niño SST anomalies are not. For the proxy ENSO index, the relationship with the observed SOI over the 20th century is linear for both phases of ENSO (Figure 5). This perhaps reflects the fact that a range of teleconnection regions are represented in the R8 proxy data.

[48] In summary, out of sixteen El Niño events identified from 1900 to 1982, thirteen (including 1978) are correctly identified by R5 and R8 and three events are missed. Only three clear false positive El Niño events (not associated with a negative SOI period in the observations) are recorded in 1930, 1967 and 1980 (R5). Out of eleven identified La Niña events from 1900 to 1982, six (including 1971) were correctly identified by the proxy ENSO indices. Four proxy-based La Niña events were falsely reconstructed, including one (1903) that is ambiguous. The proxy ENSO index also identifies the year preceding an observed La Niña as a threshold event on six occasions. The reconstructions produced here are consistent with previous studies in that they underrepresent the observed number of events. The reconstructions show higher skill in reproducing warm phase ENSO events than cold phase events.

7. Low-Frequency ENSO Variability and the IPO

[49] ENSO reconstructions should, ideally, also faithfully represent lower-frequency (decadal or greater) changes in ENSO. Both ENSO and ENSO teleconnectivity have been shown to display decadal and interdecadal variability [*Allan et al.*, 1996; *Power et al.*, 1999]. *Power et al.* [1999] show that the relationship between ENSO and Australian rainfall on interannual time scales varies on interdecadal time scales, in correspondence to changing phases of the Interdecadal Pacific Oscillation (IPO). The IPO is defined as a decadal mode of Pacific SST variability that bears pattern similarity to ENSO SST variability [*Folland et al.*, 1999; *Power et al.*, 1999] and closely resembles low-frequency ENSO in the interdecadal component of the Pacific Decadal Oscillation (PDO) [*Mantua et al.*, 1997; *Folland et al.*,

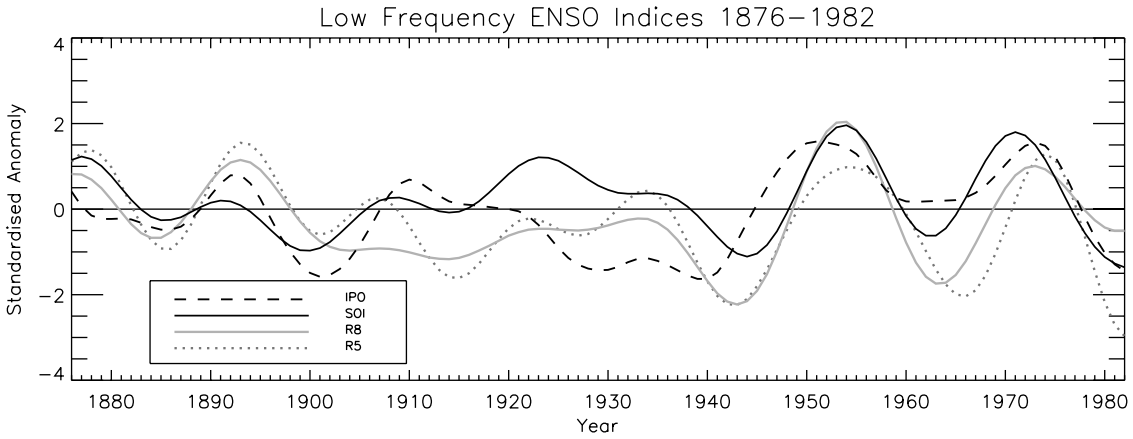

Figure 8. Low-frequency ENSO from 1876 to 1982. Proxy ENSO indices R5 and R8 are shown together with the low-frequency component of the SOI (each time series is filtered using a low-pass filter using the spectral method described by *Power et al.* [1999]) and the negative phase of the IPO.

2002; *Power et al.*, 1999]. Hence, the ability to characterize low-frequency ENSO would greatly improve the usefulness of the proxy ENSO index as a diagnostic tool for past climate.

[50] Several tree ring studies [*Hughes*, 2002; *Cook et al.*, 2004] have made note of potential limitations in the ability of climate proxies to register low-frequency climate variability. However, *Esper et al.* [2002] demonstrate that through the careful selection and treatment of tree ring chronologies, it is possible to preserve temperature variability on multicentennial time scales. Here we investigate the low-frequency variability of R8 and R5 in comparison to low-frequency ENSO. Figure 8 shows the index of the IPO over the 20th century compared to the low-frequency component of observed SOI and low-frequency R8 and R5 over the period 1876–1982. Low-frequency SOI and proxy ENSO indices have been estimated using a low-pass filter using the spectral method described by *Power et al.* [1999].

[51] The proxy indices explain 39% of the decadal scale variability shown in the instrumental SOI, with notable differences in amplitude, particularly during the first 40 years of the 20th century. Comparison between R8, the SOI and the IPO shows that the reconstruction provides a reasonable measure of IPO/PDO-like variability. The largest differences between low-frequency ENSO and the proxy indices occur during 1900–1940. The R5 reconstruction estimates greater decadal variability than any of the other indices during this period.

8. ENSO Over the Last 4 Centuries

[52] Here we describe various changes in the proxy ENSO indices over the last 450 years. Figure 9 shows the extended time series for R5 (1525–1982) and R8 (1727–1982). Figure 10 shows the low-frequency component (as defined above) of R5 and R8 for the same periods. Temporal changes in the frequency domain for R5 are shown in Figure 11, which uses a 50-year moving window to calculate the spectral power of the proxy ENSO index since 1525. Figure 11 suggests considerable amplitude and frequency modulation in ENSO over the past 4 centuries. Results for the spectral analysis are insensitive to window lengths between 30 and 80 years.

[53] There are a number of notable changes in ENSO variability evident during the reconstruction period. In particular, there are extended periods of relative quiescence in high-amplitude, interannual (~3–4 year) variability dur-

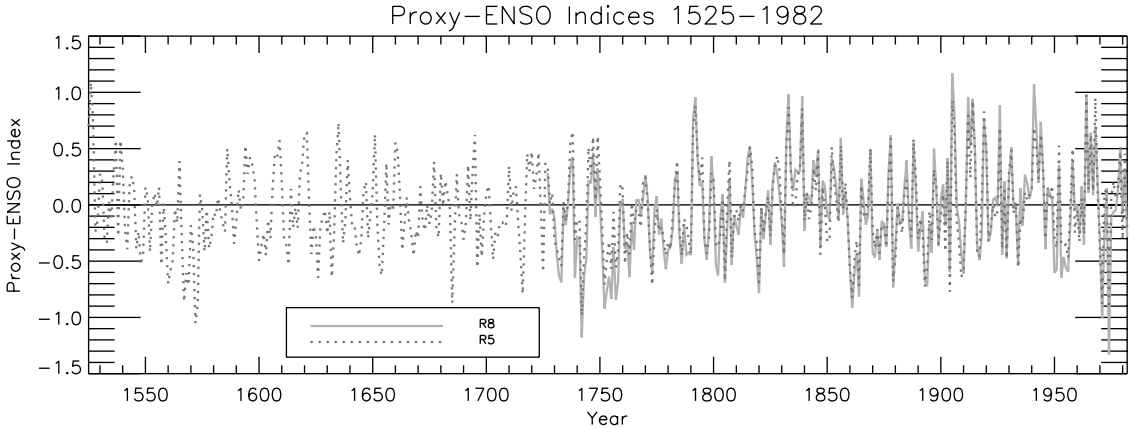

Figure 9. Proxy ENSO indices R5 (dotted) and R8 (gray) for the period 1525–1982.

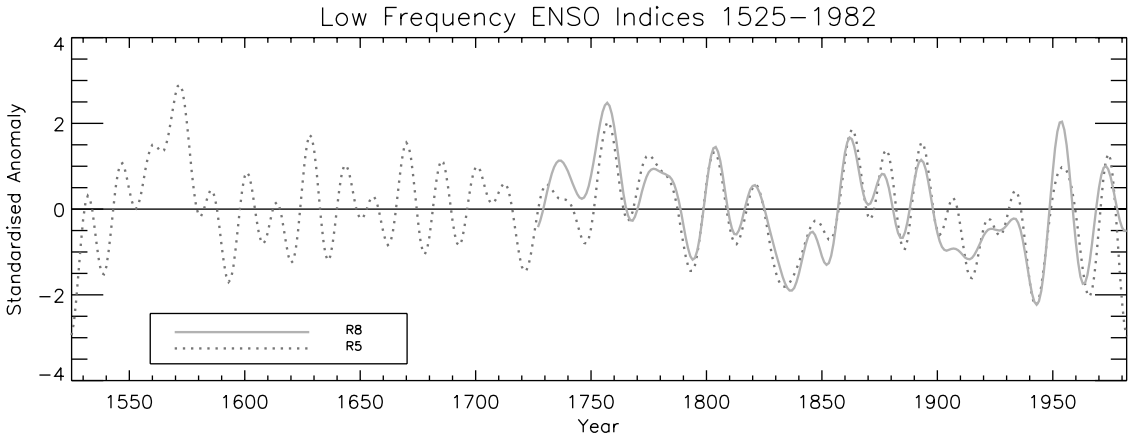

Figure 10. Low-frequency proxy ENSO indices R5 and R8 from 1525 to 1982. Each time series is low-pass filtered using the spectral method described by *Power et al.* [1999].

ing the sixteenth and early seventeenth centuries, and again during the eighteenth century. ENSO variability during these periods is dominated by interdecadal or longer time scales. The signal of higher-frequency variability, particularly as a fraction of total variability, increases from the beginning of the nineteenth century until the mid–twentieth century, near the end of our record. Very few threshold-based El Niño events (events being defined using a one standard deviation threshold, and using a moving 50-year window to determine the standard deviation) are recorded during the sixteenth century and during the last 50 years of the eighteenth century.

[54] The timing of changes suggested by the R5 index is not consistent with previous ENSO reconstructions. For example, while *Mann et al.* [2000] also noted pronounced breakdowns in internannual variability of tropical SST, these occurred during the early to mid–nineteenth century of their record. Documentary records of ENSO events, for example, *Quinn et al.* [1987], show a reasonably consistent occurrence of interannual El Niño events from 1525 to near-present. Several reasons may exist for these differences. Most obviously, the proxy network employed here differs to previous ENSO index reconstructions through the inclusion of several southwestern Pacific sites. Documentary records of El Niño events such as that of *Quinn et al.* [1987] rely on subjective classification of events, which suffer from the shortcomings associated with quantifying anecdotal information, and often have a poor correspondence with instrumental indices. For example, *Rasmusson et al.* [1995] conclude that recurrence statistics derived from the Quinn et al. compilation of El Niño events cannot be considered a reliable index of basin-scale ENSO variability. Similarly, however, the designation of events using a simple threshold in the proxy ENSO indices used here may be too simplistic to correctly identify past El Niño and La Niña occurrences. This is especially true given that the long record may be subject to low-frequency variability on multidecadal time scales that is an artifact of the analysis (as a result, for example, of by chance association between background noise in the proxy network).

[55] Dynamical studies have suggested that solar, volcanic and anthropogenic radiative forcing changes have influenced past ENSO variability, particularly a tendency toward

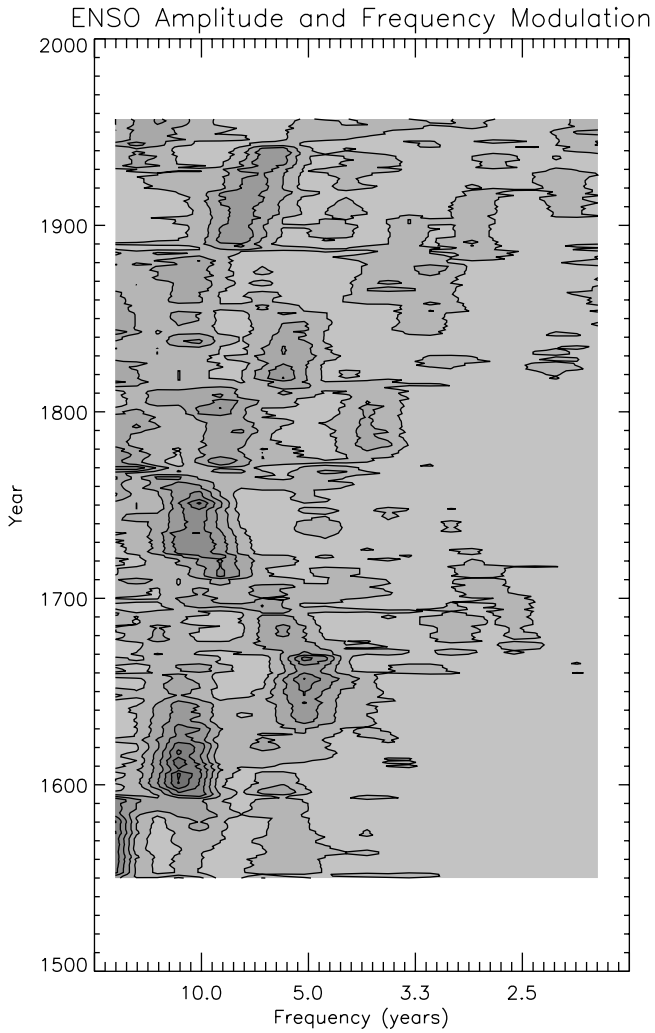

Figure 11. Hovmoller of the 50 year moving (window) power spectrum for proxy ENSO for 1525–1982. Effective bandwidth after smoothing = 2.66/N cycles/a.

El Niño–like conditions during periods of radiative cooling [*Clement et al.*, 1996; *Cane et al.*, 1997; *Mann et al.*, 2005]. However, given the complexity of the atmosphere-ocean feedbacks involved in ENSO and the inconsistency in current ENSO modeling efforts [*Collins*, 2005] causal relationships based upon the simplistic correlation of apparent changes must be viewed with circumspection. On the basis of the timing of changes in the amplitude and frequency of R5 and R8, we find it difficult to isolate any obvious synchronicity between well documented, past radiative forcing changes and changes in ENSO variability in proxy ENSO. Pronounced changes in ENSO in the late 19th/early 20th century that have been noted by previous researchers [*Stahle et al.*, 1998; *Allan*, 2000; *Trenberth and Caron*, 2000] are also not found in this study, although we do find evidence of greater high-frequency variability.

9. Summary

[56] In this study we reconstruct a proxy record of ENSO-related variability over the last 5 centuries, using a network of paleoclimate indicators spanning a broad geographic region of the Pacific. An eight-member multiproxy data set (R8), comprising two subtropical North American tree rings, two New Zealand tree rings, three western/central Pacific coral records and a single South American ice core, is used to reconstruct ENSO variability from A.D. 1727 to 1982. The tree ring and ice core records are also used in a five-member network (R5) to reconstruct a longer record of ENSO variability from A.D. 1525 to 1982. These two proxy networks differ from previous reconstructions in containing proxy sites with a distinct ENSO signal from the southwest Pacific (New Zealand tree rings and Australian corals).

[57] Our index of ENSO variability is defined simply as the time series of the leading mode of covariability from the proxy network. This approach differs to most previous studies, which have calibrated proxy ENSO variability by regressing their paleoindicators against observed 20th century indices. For ENSO, where the absolute scale of the index is meaningless, we find that such direct calibration of the proxy indicators is unnecessary. Further, using synthetic data testing and reasoning, we conclude that direct calibration of the index to 20th century observations does not significantly improve the fidelity of the proxy index and may introduce errors to the reconstruction outside of the calibration period.

[58] The time amplitude of the leading EOF from each of the proxy data sets is well correlated with the SOI, Niño3.4 SST and a combined ocean-atmosphere index (CEI) over the 20th century. Both indices R5 and R8 compare well with previously published reconstructions in terms of the proportion of common variance explained and the ability to register threshold-defined El Niño events. In common with previous efforts, there is less skill in capturing La Niña events. Both paleo-ENSO indices also reproduce the main spectral characteristics of the instrumental ENSO indices. Of the three instrumental indices investigated here (SOI, CEI and Niño3.4 SST), highest correspondence/skill is found with the composite land-ocean CEI index.

[59] The R8 ENSO index (which includes western Pacific coral records) explains a higher proportion of instrumental SOI (52%) than the R5 index (43%). We conclude, more generally, that the inclusion of proxy sites across a broader region of the Pacific provides a robust reconstruction of ENSO. This is primarily a reflection of the fact that the strength of ENSO regional teleconnections is nonstationary and that a larger network of proxies provides more degrees of freedom, thereby reducing potential errors due to site-specific biases.

[60] In terms of the reality of the extended ENSO reconstructions, a number of factors need to be considered. While covering a broad area, the network used here is still incomplete, with no sites from the far-western equatorial Pacific. Reconstructions may be expected to be more robust in the frequency domain than the amplitude domain. The ability to register individual warm/cold events is sensitive to noise in the reconstructions as well as to potential nonlinearity in the relationship between the proxies and large events. This means that attempts to characterize past changes in ENSO should not rely solely on "event capture" statistics. Changes in ENSO are perhaps more accurately gauged from the amplitude and frequency modulation of continuous, high temporal resolution indices.

[61] The apparent amplitude and frequency modulation in the R5 proxy ENSO index is suggestive of some interesting changes in ENSO over the last 4 centuries. The amplitude of high-frequency (~2–4 year) ENSO variability is relatively low during the sixteenth, early seventeenth and mid–eighteenth centuries. There are also extended periods of the record where interdecadal (~8–20 year) variability is larger than interannual variability. High-frequency variability has increased over the last 200 years compared with the preceding 250 years. However, in the context of the entire record, we find no pronounced signal of twentieth century climate change in ENSO variability. It must be noted however, that our proxy ENSO index does not extend to the period after 1982, which coincides with a period of rapid warming in global temperature. Extension of the index to the modern era will be the subject of future work.

[62] **Acknowledgments.** Many thanks to Erica Hendy (Lamont Doherty Earth Observatory) for Great Barrier Reef coral luminescence record, Pavla Fenwick (Lincoln University, New Zealand) for pink pine tree ring data, and Bruce Bauer and Connie Woodhouse (World Data Center for Paleoclimatology/National Climatic Data Center Paleoclimatology Branch) for data acquisition and assistance. The authors thank Harry Hendon, Matthew Wheeler (Bureau of Meteorology, Centre for Australian Weather and Climate Research), and Grant Beard and Robert Fawcett (Bureau of Meteorology, National Climate Centre) for useful discussions regarding methodologies for spectral and time series analysis. We thank internal reviewers Doerte Jakob and Brad Murphy (Bureau of Meteorology). We also thank two anonymous reviewers for JGR for their comments. For part of this study, J.L.G. was supported at UNSW by an Australian postgraduate award. A.M.F. was funded by the Royal Society of New Zealand Marsden Fund (contract UOA108). J.S.R. has been partly supported by the CSIRO Wealth from Oceans Flagship program.

References

Allan, R. (2000), ENSO and climatic variability in the past 150 years, in *El Niño and the Southern Oscillation: Multiscale Variability and Global and Regional Impacts*, edited by H. Diaz and V. Markgraf, pp. 3–35, Cambridge Univ. Press, Cambridge, U. K.

Allan, R., J. Lindsay, and D. Parker (1996), *El Niño Southern Oscillation and Climate Variability*, CSIRO, Melbourne, Vic., Australia.

Allan, R., C. Reason, J. Lindsay, and T. Ansell (2003), Protracted ENSO episodes and their impacts in the Indian Ocean region, *Deep Sea Res., Part II*, *50*(1213), 2331–2347.

Bath, M. (1974), *Spectral Analysis in Geophysics*, 563 pp., Elsevier Sci., Amsterdam.

Baumgartner, T., J. Michaelsen, L. Thompson, G. Shen, A. Soutar, and R. Casey (1989), The recording of interannual climatic change by high-resolution natural systems: Tree-rings, coral bands, glacial ice layers and marine varves, in *Aspects of Climate Variability in the Pacific and Western Americas*, *Geophys. Monogr. Ser.*, vol. 55, edited by D. Peterson, pp. 1–14, AGU, Washington, D. C.

Bradley, R. (1996), Are there optimum sites for global palaeotemperature reconstruction?, in *Climate Variations and Forcing Mechanisms of the Last 2000 Years*, edited by P. Jones, R. Bradley, and J. Jouzel, pp. 603–624, Springer, Berlin.

Braganza, K., J. L. Gergis, S. B. Power, J. S. Risbey, and A. M. Fowler (2008), A multi-proxy index of the El Nino Southern Oscillation, A.D. 1525–1982, *Tech. Rep. 005*, 70 pp., Cent. for Aust. Weather and Clim. Res., Bur. of Meteorol., Melbourne, Vic., Australia.

Cane, M. A., A. C. Clement, A. Kaplan, Y. Kushnir, D. Pozdnyakov, R. Seager, S. E. Zebiak, and R. Murtugudde (1997), Twentieth-century sea surface temperature trends, *Science*, *275*, 957–960, doi:10.1126/science.275.5302.957.

Cleaveland, M., D. Stahle, M. Therrell, J. Villanueva-Diaz, and B. Burns (2003), Tree-ring reconstructed winter precipitation and tropical teleconnections in Durango, Mexico, *Clim. Change*, *59*, 369–388, doi:10.1023/A:1024835630188.

Clement, A. C., R. Seager, M. A. Cane, and S. E. Zebiak (1996), An ocean dynamical thermostat, *J. Clim.*, *9*, 2190–2196, doi:10.1175/1520-0442(1996)009<2190:AODT>2.0.CO;2.

Collins, M. (2005), El Niño or La Niña-like climate change?, *Clim. Dyn.*, *24*, 89–104, doi:10.1007/s00382-004-0478-x.

Cook, E. R., and K. Peters (1981), The smoothing spline: A new approach to standardizing forest interior tree-ring width series for dendroclimatic studies, *Tree Ring Bull.*, *42*, 45–53.

Cook, E. R., C. A. Woodhouse, M. C. Eakin, D. M. Meko, and D. W. Stahle (2004), Long-term aridity changes in the western United States, *Science*, *306*, 1015–1018, doi:10.1126/science.1102586.

Crowley, T. (2000), Causes of climate change over the past 1,000 years, *Science*, *289*, 270–277, doi:10.1126/science.289.5477.270.

D'Arrigo, R., G. Jacoby, and P. Krusic (1994), Progress in dendroclimatic studies in Indonesia, *Terr. Atmos. Oceanogr. Sci.*, *5*, 349–363.

D'Arrigo, R., E. Cook, R. Wilson, R. Allan, and M. Mann (2005), On the variability of ENSO over the past six centuries, *Geophys. Res. Lett.*, *32*, L03711, doi:10.1029/2004GL022055.

Diaz, H., and V. Markgraf (2000), *El Niño and the Southern Oscillation: Multiscale Variability and Global and Regional Impacts*, Cambridge Univ. Press, Cambridge, U. K.

Diaz, H., and R. Pulwarty (1994), An analysis of the time scales of variability in centuries-long ENSO-sensitive records in the last 1000 years, *Clim. Change*, *26*, 317–342, doi:10.1007/BF01092422.

Esper, J., E. R. Cook, and F. H. Schweingruber (2002), Low-frequency signals in long tree-ring chronologies for reconstructing past temperature variability, *Science*, *295*, 2250–2253, doi:10.1126/science.1066208.

Evans, M. N., A. Kaplan, and M. A. Cane (2002), Pacific sea surface temperature field reconstruction from coral δ^{18}O data using reduced space objective analysis, *Paleoceanography*, *17*(1), 1007, doi:10.1029/2000PA000590.

Fairbanks, R., M. Evans, J. Rubenstone, R. Mortlock, K. Broad, M. Moore, and C. Charles (1997), Evaluation of climate indices and their geochemical proxies measured in corals, *Coral Reefs*, *16*, suppl., S93–S100, doi:10.1007/s003380050245.

Fenwick, P (2003), Reconstruction of past climates using pink pine (Halocarpus biformus) tree-ring chronologies, Ph.D. thesis, Soil, Plant and Ecol. Sci. Div., Lincoln Univ., Christchurch, New Zealand.

Folland, C. K., D. E. Parker, A. W. Colman, and R. Washington (1999), Large scale modes of ocean surface temperature since the late nineteenth century, in *Beyond El Nino: Decadal and Interdecadal Climate Variability*, edited by A. Navarra, chap. 4, pp. 73–102, Springer, Berlin.

Folland, C., T. Karl, J. Christy, R. Clarke, G. Gruza, J. Jouzel, M. Mann, J. Oerlemans, M. Salinger, and S. Wang (2001), Observed climate variability and change, in *Climate Change 2001: The Scientific Basis—Contribution of Working Group 1 to the Third Assessment Report of the Intergovernmental Panel on Climate Change*, edited by J. Houghton et al., pp. 99–182, Cambridge Univ. Press, Cambridge, U. K.

Folland, C. K., J. A. Renwick, M. J. Salinger, and A. B. Mullan (2002), Relative influences of the Interdecadal Pacific Oscillation and ENSO on the South Pacific Convergence Zone, *Geophys. Res. Lett.*, *29*(13), 1643, doi:10.1029/2001GL014201.

Fowler, A. M. (2008), ENSO history recorded in *Agathis australis* (kauri) tree-rings part B: 422 years of ENSO robustness, *Int. J. Climatol.*, *28*(1), 21–35, doi:10.1002/joc.1479.

Fowler, A., and G. Boswijk (2003), Chronology stripping as a tool for enhancing the statistical quality of tree-ring chronologies, *Tree Ring Res.*, *59*(2), 53–62.

Fowler, A., J. Palmer, J. Salinger, and J. Ogden (2000), Dendroclimatic interpretation of tree-rings in Agathis australis (kauri) 2: Evidence of a significant relationship with ENSO, *J. R. Soc. N. Z.*, *30*(3), 277–292.

Fowler, A., G. Boswijk, and J. Ogden (2004), Tree-ring studies on Agathis australis (kauri): A synthesis of development work on Late Holocene chronologies, *Tree Ring Res.*, *60*(1), 15–29.

Fowler, A. M., G. Boswijk, J. Gergis, and A. Lorrey (2008), ENSO history recorded in *Agathis australis* (kauri) tree-rings part A: Kauri's potential as an ENSO proxy, *Int. J. Climatol.*, *28*(1), 1–20, doi:10.1002/joc.1525.

Garcia-Herrera, R., H. F. Diaz, R. R. Garcia, M. R. Prieto, D. Barriopedro, R. Moyano, and E. Hernández (2008), A chronology of El Niño events from primary documentary sources in northern Peru, *J. Clim.*, *21*, 1948–1962, doi:10.1175/2007JCLI1830.1.

Gedalof, Z., and N. Mantua (2002), A multi-century perspective of variability in the Pacific Decadal Oscillation: new insights from tree rings and coral, *Geophys. Res. Lett.*, *29*(24), 2204, doi:10.1029/2002GL015824.

Gergis, J., and A. Fowler (2005), Classification of synchronous oceanic and atmospheric El Niño–Southern Oscillation (ENSO) events for palaeoclimate reconstruction, *Int. J. Climatol.*, *25*, 1541–1565, doi:10.1002/joc.1202.

Gergis, J., G. Boswijk, and A. Fowler (2005a), An update of modern Northland kauri (*Agathis australis*) tree-ring chronologies 1: Puketi State Forest, *N. Z. Tree-Ring Site Rep. 19*, Sch. of Geogr. and Environ. Sci., Univ. of Auckland, Auckland, New Zealand.

Gergis, J., G. Boswijk, and A. Fowler (2005b), An update of modern Northland kauri (*Agathis australis*) tree-ring chronologies 2: Trounson Kauri Park, *N. Z. Tree-Ring Site Rep. 20*, Sch. of Geogr. and Environ. Sci., Univ. of Auckland, Auckland, New Zealand.

Gergis, J., K. Braganza, A. Fowler, J. Risbey, and S. Mooney (2006), Reconstructing El Niño-Southern Oscillation (ENSO) from high-resolution palaeoarchives, *J. Quat. Sci.*, *21*(7), 707–722, doi:10.1002/jqs.1070.

Gilman, D. L., F. J. Fuglister, and J. M. Mitchell (1963), On the power spectrum of red noise, *J. Atmos. Sci.*, *20*, 182–184, doi:10.1175/1520-0469(1963)020<0182:OTPSON>2.0.CO;2.

Goodwin, I., T. van Ommen, M. Curran, and M. Mayewski (2004), Mid latitude winter climate variability in the South Indian and southwest Pacific regions since 1300 AD, *Clim. Dyn.*, *22*, 783–794, doi:10.1007/s00382-004-0403-3.

Hanley, D., M. Bourassa, J. O'Brian, S. Smith, and E. Spade (2003), A quantitative evaluation of ENSO indices, *J. Clim.*, *16*, 1249–1258, doi:10.1175/1520-0442(2003)16<1249:AQEOEI>2.0.CO;2.

Hendy, E., M. Gagan, and J. Lough (2003), Chronological control of coral records using luminescent lines and evidence for non-stationarity ENSO teleconnections in northeastern Australia, *Holocene*, *13*(2), 187–199, doi:10.1191/0959683603hl606rp.

Hendy, E., et al. (2005), Great barrier reef coral luminescence data, *IGBP PAGES/WDC-A for Paleoclimatol. Data Contrib. Ser., 2005-032*, ftp://ftp.ncdc.noaa.gov/pub/data/paleo/coral/west_pacific/great_barrier/gbr-luminescence2003.txt, Paleoclimatol. Program, Natl. Clim. Data Cent., NOAA, Boulder, Colo.

Hoerling, M. P., A. Kumar, and M. Zhong (1997), El Niño, La Niña, and the nonlinearity of their teleconnections, *J. Clim.*, *10*, 1769–1786, doi:10.1175/1520-0442(1997)010<1769:ENOLNA>2.0.CO;2.

Hughes, M. K. (2002), Dendrochronology in climatology—The state of the art, *Dendrochronologia*, *20*(1–2), 95–116, doi:10.1078/1125-7865-00011.

Jones, P., and M. Mann (2004), Climate over past millennia, *Rev. Geophys.*, *42*, RG2002, doi:10.1029/2003RG000143.

Kutzbach, J. E. (1967), Empirical eigenvectors of sea-level pressure, surface temperature, and precipitation complexes over North America, *J. Appl. Meteorol.*, *6*(5), 791–802, doi:10.1175/1520-0450(1967)006<0791:EEOSLP>2.0.CO;2.

Linsley, B., G. Wellington, and D. Schrag (2000a), Decadal sea surface temperature variability in the subtropical South Pacific from 1726 to 1997 A.D., *Science*, *290*, 1145–1149, doi:10.1126/science.290.5494.1145.

Linsley, B., et al. (2000b), Rarotonga Sr/Ca and SST reconstruction data, *IGBP PAGES/WDC-A for Paleoclimatol. Data Contrib. Ser., 2000-065*, ftp://ftp.ncdc.noaa.gov/pub/data/paleo/coral/east_pacific/rarotonga_2000b.txt, Paleoclimatol. Program, Natl. Clim. Data Cent., NOAA, Boulder, Colo.

Linsley, B., G. Wellington, D. Schrag, L. Ren, J. Salinger, and A. Tudhope (2004), Geochemical evidence from corals for changes in the amplitude and spatial pattern of South Pacific interdecadal climate variability over the last 300 years, *Clim. Dyn.*, *22*, 1–11, doi:10.1007/s00382-003-0364-y.

Lough, J. (2004), A strategy to improve the contribution of coral data to high-resolution palaeoclimatology, *Palaeogeogr. Palaeoclimatol. Palaeoecol.*, *204*, 115–143, doi:10.1016/S0031-0182(03)00727-2.

Lyon, B., and A. Barnston (2005), The evolution of the weak El Niño of 2004–2005, *U.S. CLIVAR Variations*, *3*(2), 1–4.

Mann, M. (2003), On past temperatures and anomalous late-20th century warmth, *Eos Trans. AGU*, *84*(27), 1–3, doi:10.1029/2003EO270003.

Mann, M., and J. Lees (1996), Robust estimation of background noise and signal detection in climatic time series, *Clim. Change*, *33*, 409–445, doi:10.1007/BF00142586.

Mann, M., R. Bradley, and M. Hughes (1998), Global-scale temperature patterns and climate forcing over the past six centuries, *Nature*, *392*, 779–787, doi:10.1038/33859.

Mann, M., R. Bradley, and M. Hughes (2000), Long-term variability in the El Niño/Southern Oscillation and associated teleconnections, in *El Niño and the Southern Oscillation: Multiscale Variability and Global and Regional Impacts*, edited by H. Diaz and V. Markgraf, pp. 327–372, Cambridge Univ. Press, Cambridge, U. K.

Mann, M., M. Cane, S. Zebiak, and A. Clement (2005), Volcanic and solar forcing of the tropical Pacific over the past 1000 years, *J. Clim.*, *18*, 447–456, doi:10.1175/JCLI-3276.1.

Mantua, N. J., S. R. Hare, Y. Zhang, J. M. Wallace, and R. C. Francis (1997), A Pacific decadal climate oscillation with impacts on salmon, *Bull. Am. Meteorol. Soc.*, *78*, 1069–1079, doi:10.1175/1520-0477(1997)078<1069:APICOW>2.0.CO;2.

Ortlieb, L. (2000), The documented historical record of El Niño events in Peru: An update of the Quinn record (sixteenth through nineteenth centuries), in *El Niño and the Southern Oscillation: Multiscale Variability and Global and Regional Impacts*, edited by H. F. Diaz and V. Markgraf, pp. 207–295, Cambridge Univ. Press, Cambridge, U. K.

Power, S. B., and R. Colman (2006), Multi-year predictability in a coupled general circulation model, *Clim. Dyn.*, *26*, 247–272, doi:10.1007/s00382-005-0055-y.

Power, S., F. Tseitkin, S. Torok, B. Lavery, and B. McAvaney (1998), Australian temperature, Australian rainfall, and the Southern Oscillation, 1910–1996: Coherent variability and recent changes, *Aust. Meteorol. Mag.*, *47*, 85–101.

Power, S., C. Folland, A. Colman, and V. Mehta (1999), Inter-decadal modulation of the impact of ENSO on Australia, *Clim. Dyn.*, *15*, 319–324, doi:10.1007/s003820050284.

Power, S., M. Haylock, R. Colman, and X. Wang (2006), The predictability of interdecadal changes in ENSO and ENSO teleconnections, *J. Clim.*, *8*, 2161–2180, doi:10.1175/JCLI3868.1.

Quinn, T., T. Crowley, F. Taylor, C. Henin, P. Joannot, and Y. Join (1998), A multicentury stable isotope record from a New Caledonia coral: Interannual and decadal SST variability in the southwest Pacific since 1657, *Paleoceanography*, *13*(4), 412–426, doi:10.1029/98PA00401.

Quinn, T. M., T. J. Crowley, F. W. Taylor, C. Henin, P. Joannot, and Y. Join (1999), New Caledonia coral multicentury stable isotope data, *IGBP PAGES/WDC-A for Paleoclimatol. Data Contrib. Ser. 1999-003*, ftp://ftp.ncdc.noaa.gov/pub/data/paleo/coral/west_pacific/amedee_1998.txt, Paleoclimatol. Program, Natl. Clim. Data Cent., NOAA, Boulder, Colo.

Quinn, W., and V. Neal (1992), The historical record of El Niño events, in *Climate Since A.D. 1500*, edited by R. Bradley and P. Jones, pp. 623–648, Routledge, London.

Quinn, W., D. Zopf, K. Short, and R. Yang (1978), Historical trends and statistics of the southern oscillation, El Nino and Indonesian droughts, *Fish. Bull.*, *76*(3), 663–678.

Quinn, W. H., V. T. Neal, and S. E. Antunez de Mayolo (1987), El Niño occurrences over the past four and a half centuries, *J. Geophys. Res.*, *92*, 14,449–14,461, doi:10.1029/JC092iC13p14449.

Rasmusson, E. M., and T. Carpenter (1982), Variations in tropical sea surface temperature and surface wind fields associated with the Southern Oscillation/El Niño, *Mon. Weather Rev.*, *110*, 354–384, doi:10.1175/1520-0493(1982)110<0354:VITSST>2.0.CO;2.

Rasmusson, E. M., X. Wang, and C. F. Ropelewski (1995), Secular variability of the ENSO cycle, in *Natural Climate Variability on Decade-to-Century Time Scales*, edited by D. G. Martinson et al., pp. 458–469, Natl. Acad. Press, Washington, D. C.

Stahle, D., et al. (1998), Experimental dendroclimatic reconstruction of the Southern Oscillation, *Bull. Am. Meteorol. Soc.*, *79*(10), 2137–2152, doi:10.1175/1520-0477(1998)079<2137:EDROTS>2.0.CO;2.

Thompson, L., E. Mosley-Thompson, and B. Morales Arnao (1984), El Niño–Southern Oscillation events recorded in stratigraphy of the tropical Quelccaya ice cap, *Science*, *226*, 50–52, doi:10.1126/science.226.4670.50.

Thompson, L., E. Mosley-Thompson, J. Bolzan, and B. Koci (1985), A 1500 year record of tropical precipitation in ice-cores from the Quleccaya ice cap, Peru, *Science*, *229*, 971–973, doi:10.1126/science.229.4717.971.

Thompson, L., et al. (1992), Quelccaya ice core database, *IGBP PAGES/WDC-A for Paleoclimatol. Data Contrib. Ser., 1992-008*, ftp://ftp.ncdc.noaa.gov/pub/data/paleo/icecore/trop/quelccaya, Paleoclimatol. Program, Natl. Clim. Data Cent., NOAA, Boulder, Colo.

Thompson, L., K. Henderson, E. Mosley-Thompson, and P. Lin (2000), The tropical ice-core record of ENSO, in *El Niño and the Southern Oscillation: Multiscale Variability and Global and Regional Impacts*, edited by H. Diaz and V. Markgraf, pp. 325–356, Cambridge Univ. Press, Cambridge, U. K.

Torrence, C., and G. P. Compo (1998), A practical guide to wavelet analysis, *Bull. Am. Meteorol. Soc.*, *79*, 61–78, doi:10.1175/1520-0477(1998)079<0061:APGTWA>2.0.CO;2.

Trenberth, K. (1997), The definition of El Niño, *Bull. Am. Meteorol. Soc.*, *78*, 2771–2777.

Trenberth, K., and J. Caron (2000), The Southern Oscillation revisited: Sea level pressures, surface temperatures, and precipitation, *J. Clim.*, *13*, 4358–4365, doi:10.1175/1520-0442(2000)013<4358:TSORSL>2.0.CO;2.

Trenberth, K., and T. Hoar (1996), The 1990–1995 El Niño Southern Oscillation event: Longest on record, *Geophys. Res. Lett.*, *23*(1), 57–60, doi:10.1029/95GL03602.

Trenberth, K., and T. Hoar (1997), El Niño and climate change, *Geophys. Res. Lett.*, *24*(23), 3057–3060, doi:10.1029/97GL03092.

Trenberth, K., and D. Stepaniak (2001), Indices of El Niño evolution, *J. Clim.*, *14*, 1697–1701, doi:10.1175/1520-0442(2001)014<1697:LIOENO>2.0.CO;2.

Troup, A. (1965), The Southern Oscillation, *Q. J. R. Meteorol. Soc.*, *91*, 490–506, doi:10.1002/qj.49709139009.

van Oldenborgh, G. J., and G. Burgers (2005), Searching for decadal variations in ENSO precipitation teleconnections, *Geophys. Res. Lett.*, *32*, L15701, doi:10.1029/2005GL023110.

Whetton, P., and I. Rutherfurd (1994), Historical ENSO teleconnections in the Eastern Hemisphere, *Clim. Change*, *28*, 221–253, doi:10.1007/BF01104135.

K. Braganza and S. B. Power, Centre for Australian Weather and Climate Research, Bureau of Meteorology, GPO Box 1289, Melbourne, Vic 3001, Australia. (k.braganza@bom.gov.au)

A. M. Fowler, School of Geography, Geology and Environmental Science, University of Auckland, Private Bag 92019, Auckland 1142, New Zealand.

J. L. Gergis, School of Earth Sciences, University of Melbourne, Melbourne, Vic 3010, Australia.

J. S. Risbey, Centre for Australian Weather and Climate Research, CSIRO, Hobart, Tas 7001, Australia.